
Article:
Schmitt, A.K., Perrine, A.R., Rhodes, E.J. orcid.org/0000-0002-0361-8637 et al. (1 more author) (2019) Age of Obsidian Butte in Imperial County, California, through infrared stimulated luminescence dating of Potassium Feldspar from tuffaceous sediment. California Archaeology, 11 (1). pp. 5-20. ISSN 1947-461X

https://doi.org/10.1080/1947461x.2019.1581678

Age of Obsidian Butte (Imperial County, California) through Infrared Stimulated Luminescence Dating of Potassium Feldspar from Tuffaceous Sediment

Axel K. Schmitt[a]*, Andrew R. Perrine[b], Edward J. Rhodes[b,c], Christian Fischer[d]

[a]Institut für Geowissenschaften, Universität Heidelberg, Heidelberg, Germany; [b]Department of Earth, Planetary, and Space Sciences, University of California, LosAngeles, USA; [c]Department of Geography, The University of Sheffield, Sheffield, United Kingdom; [d]Cotsen Institute of Archaeology, University of California, Los Angeles, USA

*corresponding author (email: axel.schmitt@geow.uni-heidelberg.de)

Age of Obsidian Butte (Imperial County, California) through Infra-red Stimulated Luminescence Dating of Potassium Feldspar from Tuffaceous Sediment

Obsidian Butte volcano is an important lithic source for obsidian, and artefacts from this location are distributed across archaeological sites in southern California and adjacent parts of northern Mexico. Here, we used drill-core material for infra-red stimulated luminescence (IRSL) dating of potassium feldspar extracted from tuffaceous sediment directly underlying obsidian-bearing lava from Obsidian Butte. In addition, a core sample from lacustrine sediment below the tuffaceous sedimentary unit was dated by the same method. Stratigraphically consistent ages between 2.51±0.32 ka (1 sigma uncertainty; average of two tuffaceous sediment samples; ka = kiloannum = 1000 years) and 4.39±0.49 ka (lacustrine sediment sample) were obtained. This constrains the eruption and earliest availability of the lithic resource of Obsidian Butte to 490 BCE (with uncertainty limits of ±320 years at ~68% confidence, and ±640 years at ~95% confidence). Since then, it would have been accessible during intermittent desiccation of Lake Cahuilla. This new date re-defines obsidian from Obsidian Butte as a maker for the late Prehistoric period.

Keywords: Geochronology; Obsidian; Volcanism; Late Holocene; Paleoclimate; Lake Cahuilla; California; Prehistory

Edad de Obsidian Butte (Imperial County, California) a través de fechamiento de Feldespato Potásico por medio de Luminiscencia Estimulada por Infrarrojo de Sedimentos Tobáceos

El volcán Obsidian Butte es una fuente lítica importante de obsidiana, y artefactos de esta localidad están distribuidos a lo largo de sitios arqueológicos al sur de California y partes adyacentes del norte de México. Aquí, utilizamos material de núcleos de perforación para el fechamiento de feldespato potásico por medio de luminiscencia estimulada por infrarrojo (IRSL, por sus siglas en inglés) extraídos de sedimentos tobáceos que subyacen directamente a lava con obsidiana proveniente de Obsidian Butte. Adicionalmente, una muestra de núcleo de sedimentos lacustres ubicada por debajo de los sedimentos tobáceos fue fechada por el mismo método. Fueron obtenidas edades estratigráficamente consistentes entre 2.51±0.32 ka (incertidumbre de 1 sigma; promedio de dos muestras de sedimentos tobáceos; ka = kiloannum = 1000 años) y 4.39±0.49 ka (muestra de sedimento lacustre). Esto restringe a la erupción y la disponibilidad más temprana del recurso lítico de Obsidian Butte a 490 BCE (con límites de incertidumbre de ±320 años al ~68% de confianza, y ±640 años al ~95% de confianza). Desde entonces, habría sido accesible durante la desecación intermitente del lago Cahuilla. Este nuevo fechamiento redefine a la obsidiana de Obsidian Butte como un marcador para el periodo Prehispánico tardío.

Palabras clave: Geocronología; Obsidiana; Volcanismo; Holoceno Tardío; Paleoclima; Lago Cahuilla; California; Prehistoria

Introduction

Obsidian Butte (Imperial County, California) is a major source for lithic artifacts in the Colorado Desert and adjacent regions of southern Alta California and northern Baja California (Fig. 1). A regional dominance of the Obsidian Butte source during the late Prehistoric versus Coso volcanic field obsidian (i.e. Sugarloaf and West Sugarloaf domes) during the early to middle Archaic periods has long been noted (e.g,, Hughes and True 1986; Panich et al. 2017), but any interpretation of these spatio-temporal distribution patterns must first satisfy the criterion of geologic availability. Especially for the Obsidian Butte source, this has long remained poorly defined.

Obsidian Butte comprises several outcrops of rhyolitic lava flows or domes, which are part of a ~7 km long NE-SW trending lineament of several small rhyolite volcanoes that are collectively termed the Salton Buttes (Robinson et al. 1976; Wright et al. 2015). These volcanoes are located in an extensional basin which experienced multiple filling and desiccation cycles by ancient Lake Cahuilla during the late Holocene (e.g., Waters 1983; Rockwell and Sieh 1994; Philibosian et al. 2011). At an elevation of -40 m below sea-level (mbsl), Obsidian Butte would have been inundated during high-stands of Lake Cahuilla, and thus would have been intermittently inaccessible for procuring lithic raw materials. Equally important for the geologic availability of Obsidian Butte materials is its eruption age. Recent geochronologic studies indicated that the Salton Buttes erupted during late Holocene times (Schmitt et al. 2013; Wright et al. 2015), superseding earlier and less precise dates suggesting a pre-Holocene eruption age (e.g., Muffler and White 1969; Friedman and Obradovich 1981). New, late Holocene eruption ages for the Salton Buttes have triggered increased attention of agencies monitoring volcanic and seismic hazards in the region, but

uncertainty remains regarding the eruption age of Obsidian Butte, the only identified source of obsidian used in an archaeological context among the Salton Buttes (Hughes 1986). Existing geochronologic constraints have limitations: (1) recent (U-Th)/He zircon dates for Red Hill (Schmitt et al. 2013) yielded a late Holocene age, but no data were obtained for Obsidian Butte; (2) available $^{40}Ar/^{39}Ar$ age for Obsidian Butte (Wright et al. 2015) are comparatively imprecise; (3) U-Th zircon ages (Wright et al. 2015) only provide a maximum eruption age because of a potential hiatus between zircon crystallization and eruption; and (4) reconstructed magnetic pole positions (Wright et al. 2015) scatter outside analytical uncertainties, possibly due to post-emplacement deformation that can obscure their age significance.

To resolve these ambiguities regarding the eruption age of Obsidian Butte and to provide a firm maximum age (terminus post quem) for the eponymous obsidian source, we have carried out Infra-red Stimulated Luminescence (IRSL) dating of K-feldspar from drill-core segments in a geothermal exploration well (Union Oil Company of California, 86-2) penetrating a sequence of Obsidian Butte lava, pumice, tuffaceous silt- and sandstone, and non-volcanic weakly indurated sandstone. K-feldspar crystals originate from the detrital fraction in three depth intervals of well 86-2, two of which represent volcaniclastic sediments with aphyric pumice typical for Obsidian Butte, and one is an underlying sandstone which lacks pumice. These detrital K-feldspar crystals are well-suited for IRSL dating (Rhodes 2015), in contrast to primary volcanic phenocrysts (e.g., Rhodes 2011), especially when K-feldspar phenocrysts are scarce such as in aphyric pumice and the lava of Obsidian Butte. Our study provides stratigraphically consistent age estimates that agree with previous (indirect) age constraints, suggesting rapid emplacement of the Salton Buttes (Schmitt et al. 2013;

Wright et al. 2015). Based on these results, maximum ages can now be firmly defined for all archaeological deposits containing lithic artifacts sourced from Obsidian Butte.

Geologic background and well stratigraphy

The Salton Buttes comprise a chain of five volcanic edifices (from NE to SW: Mullet Island, North and South Red Hill, Rock Hill, Obsidian Butte) which consist of largely aphyric rhyolite lava and minor amounts (in the case of South Red Hill and Obsidian Butte) of volcaniclastic deposits (Robinson et al. 1976; Wright et al. 2015). Among these volcanoes, only Obsidian Butte exposes black obsidian (Robinson et al. 1976). At elevations ranging from -38 to -56 mbsl these small volcanoes rise a few tens of meters above the fluctuating water level of the modern Salton Sea causing ambiguities in the use of "hill" vs. "island" in the names of some of the Salton Buttes. The Salton Sea originated in 1905 from a breach in the local irrigation network, causing Colorado River water to fill the basin for ca. two years until dams could be restored, and it has been maintained by irrigation runoff since then. In contrast to man-made Salton Sea, the basin fill of ancient Lake Cahuilla reached high-stands of +12 meters above sea-level (masl; Waters 1983), which would cover the Obsidian Butte and the other Salton Buttes volcanoes. Lacustrine sediment derived from the Colorado River abounds in surface deposits surrounding the Salton Buttes. Mud pots and fumaroles tracing the NW-SE trending regional faults of the San Andreas fault systems (Lynch and Hudnut 2008), including active steam vents on North Red Hill (Lynch and Adams 2014) attest to the youthful age of volcanism.

The original morphology of Obsidian Butte has been largely obliterated by quarrying and geothermal exploration, but based on the early description in Kelley and

Soske (1936), it consisted of marginal obsidian lava ridges surrounding a central hill of pumiceous deposits. Whereas the central dome-like structure has been completely removed by quarrying, some of the marginal obsidian ridges have remained intact (Fig. 1). The preservation of archaeological materials, despite the abundance of fresh-looking obsidian fragments littering the ground, remains unclear.

Geothermal exploration well Union Oil Company of California 86-2 provides additional insight into the subsurface structure of Obsidian Butte (California Division of Mines and Geology, 2011; this study). Samples of core and cuttings from well 86-2 were stored at the Union Oil storage facility in El Centro until the geothermal division was shut down, at which point remaining samples were salvaged by Prof. Wilfred Elders (W. A. Elders, 2010, personal communication) and ultimately transferred to one of us (AKS). The well-head was at an elevation of -65 mbsl, total well depth is 91.5 m, and original core recovery was 100%. However, only ~6 m (~6.6%) of the total core and cuttings spanning a depth range from 0 to 73 m are currently preserved (Fig. 2). Three main lithostratigraphic units were distinguished in well 86-2 using the nomenclature for volcaniclastic sediments in Busby et al. (2017), and reinterpreting the original well log (State of California, Department of Conservation, Division of Oil, Gas, and Geothermal Resources 2017): Unit 1 (igneous; 0 – 41 m depth), Unit 2 (41 – 60 m), and Unit 3 (60 – 91.5 m; well bottom). Due to incomplete sample coverage, no contacts between lithostratigraphic units are available in the preserved intervals, and total thickness estimates are therefore only approximate. Unit 1 consists primarily of lithophysae-rich obsidian, massive black obsidian (mostly near the top and bottom), and intervals of microcrystalline rhyolite (mostly near the bottom). Intercalated intervals of pumiceous rhyolite, autobrecciated rhyolite lava, and tuffaceous sediment are present in minor amounts (Fig. 2). Lithostratigraphic Unit 2 comprises mostly moderately

consolidated tuffaceous sediment with ~10-30 % silky-white, aphyric, tubular pumice lapilli in an ochre silt- to sand-grained matrix (Fig. 2). It is separated from overlying Unit 1 by a small interval of laminated mudstone at 43.2 m. Lapilli-sized obsidian lithic fragments are present in the upper intervals of Unit 2, but are lacking in its lower intervals. Unit 3 begins with a small interval of laminated mudstone at 60 m depth, but deeper intervals mostly consist of moderately consolidated fine to very-fine sand-sized clastic sediment lacking pumice (Fig. 2). The sediment has a roughly arkosic composition; grains are well rounded and quartz has a frosted appearance indicative of sedimentary transport.

The presence of pumice with identical texture and mineralogical composition in Unit 1 and Unit 2 is strong evidence that both units are genetically closely related. Similar tuffaceous clay- to sand-sized deposits are present at South Red Hill along with deposits of accretionary lapilli. Unit 2 thus represents the initial phreatomagmatic eruption stage of Obsidian Butte, which due to the aridic climate of the region likely involved magma interaction with lake water rather than groundwater. This suggest that the basin was filled at the time of the Obsidian Butte eruption. The initial phreatomagmatic phase was followed by effusive emplacement of degassed rhyolite lava forming the rocks of Unit 1. The basal Unit 3 in well 86-2 is interpreted as Colorado River-derived sediments, which were deposited in the lacustrine environment of Lake Cahuilla.

Sampling, preparation and luminescence measurement

Three core samples approximately 10 cm long and 7.5 cm in diameter were selected for IRSL analysis (Table 1). Samples are identified by the well designation “86-2”,

followed by their depth given in feet as is conventional for well-logs, but converted into metric depth in plots (Fig. 2). Samples 86-2-148.3 and 86-2-162.8 (45.2 and 49.6 m depth, respectively) are from tuffaceous silt- and sandstone of Unit 2, and sample 86-2-239.0 (72.8 m depth) from fine to very-fine sandstone of Unit 3. All following procedures were carried out under controlled laboratory lighting conditions (Rhodes, 2011). The original drill core surfaces were painted black with spray paint, and trimmed using a hacksaw to remove any light-contaminated materials on the outside of the cores. The remaining 2-3 cm diameter interiors of the cores were then gently disaggregated and wet sieved to sort by grain size. The size fraction of 175 to 200 μm was then treated with dilute HCl to dissolve carbonates, and gravity separated with a lithium metatungstate heavy liquid of density 2.565 $g.cm^{-3}$ to separate potassic feldspar grains. Finally, a brief dilute HF treatment (10% HF for 10 mins.) was performed to dissolve dark grain coatings on the K-feldspar fraction and remove the outer alpha irradiated layer. Individual grains were then transferred into measurement positions on the sample tray of a Risø TL-DA-20 D automated luminescence reader.

IRSL measurements followed the single grain protocol detailed in Rhodes (2015) that was extensively tested by comparison with independent age controls. K-feldspar was selected owing to low quartz sensitivity in many parts of southern California (Lawson et al., 2012). A post-IR IRSL approach was used, in order to access a luminescence signal with good thermal stability characteristics measured using a single aliquot regenerative-dose (SAR) protocol. For each grain, a series of SAR cycles was measured with different regenerative doses. Within each SAR cycle, following the regenerative dose, a preheat of 250°C for 60 s was administered. After this, the IRSL measurement was performed at 50°C for 2.5 s for each grain to remove the least stable IRSL signal components, followed by a second IRSL measurement at 225°C for the

same duration. It is the initial 0.5 s of this second, or post-IR IRSL signal at 225°C that was used for age estimation. Stimulation was performed at 90% power with a 150 mW IR laser emitting at 830 nm filtered with a RG780 interference filter. Following a standard test dose of around 9 Gy, repeat IRSL measurements at both 50 and 225°C were made to allow correction for sensitivity change. Each SAR cycle ended with a "hot bleach" IRSL treatment for 40 s at 290°C using IR stimulation from light emitting diode clusters. Including measurement of the natural dose, a total of seven SAR cycles was performed.

Inductively-coupled plasma (ICP) optical emission spectroscopy (ICP-OES) was carried out to determine K abundances on aliquants of the dated sediment, and ICP mass spectrometry (ICP-MS) for Th, and U abundances. These values were used to determine external dose rates. In addition, trace element analyses of aphyric pumice from a section slightly above that of sample 86-2-148.3 was carried out to confirm that the dated segment is chemically equivalent to the overlying lava flow from which obsidian was procured. In addition, selected trace elements were analyzed in rock powders filled to >1 cm in a plastic cup with a thin film bottom using a Thermo Scientific Niton® XL3t GOLDD+ portable X-ray fluorescence spectrometer (p-XRF) at the Cotsen Institute of Archaeology at UCLA. Data are presented along with pXRF analyses of USGS rock reference powders (Table 2).

Results

Equivalent dose distributions for the three samples (Fig. 3) show a variety of responses. The uppermost sample (86-2-148.3) was measured in considerable detail (n = 104 single grain age determinations). It displays several clusters of apparent single grain age

estimates around 2.5, 6, and 10 ka (Fig. 3a) plus a minor cluster at ca. 40 ka (not shown in Fig. 3a). We interpret this multi-modal distribution as representing different events when grains were transported and exposed to light, the youngest of these corresponding to the depositional age of this sediment. Many grains provide older apparent age estimates, indicating that they were not exposed to sufficient light to reduce their luminescence signal to a low level at the time of deposition. Despite this, the sample is moderately well-bleached, with 32% of grains providing equivalent dose values consistent with the shared minimum age estimate (assuming an overdispersion value of 15% for all three analyses; Rhodes, 2015). The criterion for assessing internal consistency for each grain is based on its equivalent dose value and uncertainty using the same statistical test as applied within the central age model to estimate an overdispersion value (OD) from a single well-bleached population (Galbraith et al., 1999). In the procedure applied here, we assume OD = 15% for all three analyses based on theoretical considerations of overdispersion caused by variations in beta dose rate at the scale of individual grains (Nathan et al., 2003), and from experience of quartz single grain distributions (Rhodes et al., 2010) and well-bleached K-feldspar single grains measured using the same post-IR IRSL protocol (Rhodes, 2015). As we are searching for the equivalent dose that corresponds to the depositional age from a mixture of well-bleached and not well-bleached grains, and therefore expect age over-estimates from some grains, we assess the distance from each grain to the weighted mean (using natural log values) of the whole remaining population, and in turn reject the grain with the highest positive deviation (i.e. age over-estimate) in sigma units (the difference divided by the OD-adjusted uncertainty value for that grain) until the statistical test presented by Galbraith (1999; equation 23) falls to zero. This indicates that the remaining population of grains has a variance consistent with the magnitude of the individual OD-adjusted

uncertainties on each value.

Using the same procedure, the second sample, (86-2-162.8) provides a similar depositional age estimate; several higher values are interpreted as grains not fully exposed at the time of last transport and deposition. Fewer grains were measured for this and the lowermost sample, owing to limited yields of suitably sized K-feldspar grains in the available small core samples. The second sample is well-bleached, with 52% of grains consistent with the shared minimum value (Fig. 3b). The lowermost sample (86-2-239.0) suffered from very low yields, and we obtained results from only seven K-feldspar grains (Fig. 3c). In our analysis, we have rejected one higher age estimate plus one lower value which we interpret as an intrusive grain which may have entered the sample during the coring procedure. Albeit the five remaining grains yield an internally consistent age estimate, the result for 86-2-239.0 is not very reliable due to the low yield, and we consequently treat this age estimate with caution.

Based on the equivalent dose, and the internal (12 wt.% K assumed for K-feldspar) and external sediment dose rates determined using ICP-OES for K concentration, and ICP-MS for Th, and U abundances, IRSL ages of 2.46±0.40 ka (sample 86-2-148.3), 2.59±0.27 ka (86-2-162.8), and 4.39±0.49 ka (86-2-239.0) were obtained (1 sigma uncertainties; Table 1). The cosmic dose is negligible due to the depth of the samples. Moisture contents were fixed to 0.15, typical for water contents of wet sediment. The two shallow samples from Unit 2 yielded indistinguishable ages, and due to the textural and compositional similarity of the deposit (both containing abundant lapilli-sized pumice) it is reasonably assumed that both were deposited within the same brief time interval. Both ages are therefore combined, providing a weighted average age of 2.51±0.32 ka (or 490±320 BCE based on the 2013 analysis year). The tentative age

for the sample from Unit 3 significantly predates the age of Unit 2 by ca. 1900 years. Given the top of Unit 3 and the depth of sample 86-2-239.0, an integrated sedimentation rate of ~7 mm/a is calculated, which agrees well within uncertainty with a ~5 mm/a sedimentation rate determined for Lake Cahuilla in the northern part of the basin (Philibosian et al. 2011).

The lapilli-sized aphyric pumice from well 86-2 (sample 86-2-140.4) is chemically similar from obsidian from the near-surface obsidian penetrated in well 86-2, with identical Rb and Zr abundances (Table 2; Fig. 4). Sr abundance is slightly elevated in 86-2-140.4, possibly due to a hotter magmatic temperature and less plagioclase fractionation compared to late erupted lava (Table 2; Fig. 4).

Discussion and conclusions

Single grain post-IR IRSL K-feldspar age estimates were obtained for tuffaceous sediment directly underlying Obsidian Butte lava. The chemical similarity between pumice from lithostratigraphic Unit 2 and the overlying lava (Unit 1) underscores that the IRSL age for volcaniclastic sediment dates the same eruption that emplaced Obsidian Butte lava, the only known source for prehistoric toolstone material among the Salton Buttes (Hughes 1986). The presence of obsidian lithics in tuffaceous sediment of Unit 2 indicates that the eruption continuously progressed from an initial explosive phreatomagmatic stage to a subsequent effusive stage (Unit 1). Effusive emplacement of lava as plugs and small surficial spires reached, based on available well-logs, a maximum thickness of 86.9 m. The internal structure of Obsidian Butte is broadly consistent with that of other rapidly cooled rhyolite lava flows (e.g., Manley and Fink, 1987; Hughes and Smith, 1993; Shackley, 2005). The obsidian-rich upper parts of this

flow became accessible to humans after the eruption ended, provided that lake levels were sufficiently low (below -40 mbsl). The widespread use of obsidian from Obsidian Butte in southern California and northern Baja California during the late Prehistoric indicates that this was ultimately the case (e.g., Hughes and True 1986; Panich et al. 2017). Conversely, the absence of artifacts from Obsidian Butte in the archaeological record prior to ca. 500 BCE cannot be cited as evidence for Lake Cahuilla high-stands during the early-mid Holocene, because this would predate the eruption.

The IRSL K-feldspar age for Obsidian Butte eruption (2.51±0.32 ka; this study) and recently published geochronologic constraints show excellent agreement (Fig. 5). Despite its young age, (U-Th)/He zircon dating of Red Hill volcano (2.48±0.94 ka; Schmitt et al. 2013) was possible due to the presence of cognate granite xenoliths which yielded zircon crystals sufficiently large to be precisely dated by this method. Because of rapid diffusion of He in zircon at magmatic temperatures, (U-Th)/He zircon geochronology dates eruptive cooling, even though zircon crystallization often significantly predates eruption (e.g., Danišík et al. 2016). The agreement between eruption ages for Obsidian Butte and Red Hill suggests coeval emplacement, although the data are permissive of minor (ca. <500 a) offsets between eruptions, which is suggested by small heterogeneities in magnetic orientation for different Salton Buttes domes (Wright et al. 2015). U-Th zircon rim ages for zircon from Obsidian Butte rhyolite lava (2.86±0.96 ka; Wright et al. 2015) date crystallization in the magma reservoir due to extremely sluggish diffusion of tetravalent Th and U in zircon even at magmatic temperatures (e.g., Danišík et al. 2016). The indistinguishable U-Th zircon rim crystallization ages and IRSL K-feldspar eruption ages imply that zircon continued to crystallize essentially until the time of eruption, although U-Th zircon interior ages indicate that crystallization initiated 1000's of years before eruption (Schmitt and

Vazquez 2006; Schmitt et al. 2013). $^{40}Ar/^{39}Ar$ anorthoclase and obsidian ages for Obsidian Butte (weighted mean plateau ages of 4.9±2.0 and 5.8±2.0 ka; (Wright et al. 2015) are consistent with a late Holocene eruption of Obsidian Butte, but the marginally older ages may indicate the presence of unsupported ^{40}Ar in the dated materials. Paleomagnetic ages for Obsidian Butte of ca. 2.0±0.2 ka (Wright et al. 2015) overlap with the IRSL K-feldspar ages within two-sigma uncertainties, and also support a younger eruption age than indicated by (comparatively imprecise) $^{40}Ar/^{39}Ar$ geochronology.

Given the currently achievable age resolution, the Obsidian Butte lithic source could only have become available to humans after ca. 500 BCE (Fig. 4). The availability of the Obsidian Butte source would thus fall mostly within the late Prehistoric period (Fig. 5), albeit accessibility might have been restricted to periods when Lake Cahuilla was either absent or only present below -40 m. Therefore, the presence of Obsidian Butte artefacts provides a firm terminus post quem for their archaeological context. Reconnaissance review of reports for archaeological sites in Southern California describing protracted human presence and a well-constrained chronostratigraphy (based on available ^{14}C dates after recalculation using the current calibration curve) determined a time interval from ca. 510 BCE to 640 CE for the earliest use of the Obsidian Butte lithic source (Kyle 1996, cited in Schmitt et al., 2013; see also McDonald 1992 for Indian Hill). While this is broadly consistent with the earliest possible geologic availability of obsidian from Obsidian Butte, we caution that there has not yet been a systematic assessment of the temporal patterns of its use. Such a study should also account for potential misidentification of Obsidian Butte (e.g., due to confusion with fused shale in some archaeological assemblages from Orange County,

California; Fig. 1), which may have affected some older reports of its use in an early Prehistoric context (Hughes and Peterson 2009).

In conclusion, we have confirmed and refined evidence for the comparatively late geologic availability of volcanic lithic resources from Obsidian Butte by dating its eruption to 490 BCE (with uncertainty limits of ±320 years at ~68% confidence, and ±640 years at ~95% confidence). Accessibility of this source was subsequently modulated by intermittent inaccessibility during periods of Lake Cahuilla high-stands, which are conceivably related to climate fluctuations because diversion of the Colorado River to fill Lake Cahuilla appears more likely during wet periods (Rockwell et al., 2018). Based on the widespread use of obsidian from Obsidian Butte, this material is an important archaeological age and potential climate marker.

Acknowledgements: Wilfred Elders kindly provided samples from geothermal well Union Oil Company of California 86-2. Janet C. Harvey is thanked for generating the LiDAR map of Obsidian Butte. Alejandro Cisneros provided the Spanish abstract. Wendy Teeter from the Cotsen Institute of Archaeology at UCLA is thanked for support during planning and execution of the project. Comments on an earlier version by M. Steven Shackley are appreciated, as are the constructive reviews by Scott Johnston and two anonymous reviewers.

References:

Brown, ND, EJ Rhodes, JL Antinao and EV McDonald

2015 Single-grain post-IR IRSL signals of K-feldspars from alluvial fan deposits in Baja California Sur, Mexico. Quaternary International 362:132-138.

Busby, Cathy J, Yoshihiko Tamura, Peter Blum, Gilles Guèrin, Graham DM Andrews, Abigail K Barker, Julien LR Berger, Everton M Bongiolo, Manuela Bordiga and Susan M DeBari

2017 The missing half of the subduction factory: shipboard results from the Izu rear arc, IODP Expedition 350. International Geology Review:1-32.

Danišík, Martin, Axel K Schmitt, Daniel F Stockli, Oscar M Lovera, István Dunkl and Noreen J Evans

2016 Application of combined U-Th-disequilibrium/U-Pb and (U-Th)/He zircon dating to tephrochronology. Quaternary Geochronology.

Friedman, Irving and John Obradovich

1981 Obsidian hydration dating of volcanic events. Quaternary Research 16(1):37-47.

Galbraith, Rex F, Richard G Roberts, Geoff M Laslett, Hiroshi Yoshida and Jon M Olley

1999 Optical dating of single and multiple grains of quartz from Jinmium rock shelter, northern Australia: Part I, experimental design and statistical models. Archaeometry 41(2):339-364.

Hughes, Richard E

1986 Trace Element Composition of Obsidian Butte, Imperial County, California. Bulletin of the Southern California Academy of Sciences 85(1):35-45.

1988 The Coso Volcanic Field reexamined: implications for obsidian sourcing and hydration dating research. Geoarchaeology 3(4):253-265.

Hughes, Richard E and Delbert L True

1986 Perspectives on the Distribution of Obsidians in San Diego County, California. North American Archaeologist 6(4):325-339.

Hughes, Richard E. and Polly Peterson

2009 Trace element analysis of fused shale. California Archaeology 1(1):29-53.

Hughes, Richard E. and Robert L. Smith

1993 Archaeology, Geology, and Geochemistry in Obsidian Provenance Studies. In Scale on Archaeological and Geoscientific Perspectives, edited by J.K. Stein and A.R. Linse, pp. 79-91. Geological Society of America Special Paper 283. Boulder, Colorado.

Kelley, Vincent C. and Joshua Lawrence Soske

1936 Origin of the Salton volcanic domes, Salton Sea, California. Journal of Geology 44(4):496-509.

Kyle, Carolyn E

1996 A 2,000 year old milling tool kit from CA-SDI-10148, San Diego, California. Pacific Coast Archaeological Society Quarterly 32(4):76-87.

Lawson, Michael J, Belinda J Roder, Dallon M Stang and Edward J Rhodes

2012 OSL and IRSL characteristics of quartz and feldspar from southern California, USA. Radiation Measurements 47(9):830-836.

Lynch, David K and Paul M Adams

2014 Hot Volcanic Vents on Red Island, Imperial County, California. Proceedings of the Proceedings of the 2014 Desert Symposium (R. Reynolds, ed.):117-120.

Lynch, David K and Kenneth W Hudnut

2008 The Wister Mud Pot Lineament: Southeastward Extension or Abandoned Strand of the San Andreas Fault? Bulletin of the Seismological Society of America 98(4):1720-1729.

Manley, Curtis R and Jonathan H Fink

1987 Internal textures of rhyolite flows as revealed by research drilling. Geology 15(6):549-552.

McDonald, Alison Meg

1992 Indian Hill Rockshelter and Aboriginal Cultural Adaptation in Anza-Borrego Desert State Park, Southeastern California, University of California, Riverside.

Muffler, L. J. Patrick and Donald E. White

1969 Active metamorphism of upper Cenozoic sediments in the Salton Sea geothermal field and the Salton Trough, southeastern California. Geological Society of America Bulletin 80(2):157-182.

Nathan, RP, PJ Thomas, M Jain, AS Murray and EJ Rhodes

2003 Environmental dose rate heterogeneity of beta radiation and its implications for luminescence dating: Monte Carlo modelling and experimental validation. Radiation Measurements 37(4-5):305-313.

Panich, Lee M, M Steven Shackley and Antonio Porcayo Michelini

2017 A Reassessment of Archaeological Obsidian from Southern Alta California and Northern Baja California. California Archaeology 9(1):53-77.

Philibosian, Belle, Thomas Fumal and Ray Weldon

2011 San Andreas fault earthquake chronology and Lake Cahuilla history at Coachella, California. Bulletin of the Seismological Society of America 101(1):13-38.

Rhodes, Edward J

2011 Optically stimulated luminescence dating of sediments over the past 200,000 years. Annual Review of Earth and Planetary Sciences 39:461-488.

2015 Dating sediments using potassium feldspar single-grain IRSL: initial methodological considerations. Quaternary International 362:14-22.

Rhodes, Edward J, Patricia C Fanning and Simon J Holdaway

2010 Developments in optically stimulated luminescence age control for geoarchaeological sediments and hearths in western New South Wales, Australia. Quaternary Geochronology 5(2-3):348-352.

Robinson, P. T., W. A. Elders and L. J. P. Muffler

1976 Quaternary volcanism in the Salton Sea geothermal field, Imperial Valley, California. Geological Society of America Bulletin 87(3):347-360.

Rockwell, Thomas K, Aron J Meltzner and Erik C Haaker

2018 Dates of the Two Most Recent Surface Ruptures on the Southernmost San Andreas Fault Recalculated by Precise Dating of Lake Cahuilla Dry Periods. Bulletin of the Seismological Society of America.

Rockwell, TK and K Sieh

1994 Correlation of large earthquakes using regional lacustrine stratigraphy, examples from the Salton Trough, California. Proceedings of the Geol. Soc. Am. Abstr. Programs 26.

Schmitt, AK and JA Vazquez

2006 Alteration and remelting of nascent oceanic crust during continental rupture: Evidence from zircon geochemistry of rhyolites and xenoliths from the Salton Trough, California. Earth and Planetary Science Letters 252(3):260-274.

Schmitt, Axel K, Arturo Martín, Daniel F Stockli, Kenneth A Farley and Oscar M Lovera

2013 (U-Th)/He zircon and archaeological ages for a late prehistoric eruption in the Salton Trough (California, USA). Geology 41(1):7-10.

Shackley, M Steven

1998 Gamma rays, x-rays and stone tools: some recent advances in archaeological geochemistry. Journal of Archaeological Science 25(3):259-270.

2005 Obsidian: geology and archaeology in the North American Southwest. University of Arizona Press.

2017 Obsidian Butte. Electronic document, http://www.swxrflab.net/obsbutte.htm, accessed July 31, 2018

Society for California Archaeology

2018 Glossary of Terms. Electronic document, https://scahome.org/about-ca-archaeology/glossary-of-terms/chronological-and-cultural-units, accessed July 31, 2018

State of California, Department of Conservation, Division of Oil, Gas, and Geothermal Resources

2017 GeoSteam - Query Geothermal Well Records, Production and Injection Data Electronic document, http://geosteam.conservation.ca.gov/WellRecord/02590662/log.pdf, accessed December 28, 2017

U.S. Geological Survey

2016a Geochemical Reference Materials and Certificates. Electronic document, https://crustal.usgs.gov/geochemical_reference_standards/powdered_RM.html, accessed July 31, 2018

2016b LiDAR of the Salton Sea. Electronic document, https://www2.usgs.gov/saltonsea/LiDAR.html, accessed December 28, 2017

Waters, Michael R

1983 Late Holocene lacustrine chronology and archaeology of ancient Lake Cahuilla, California. Quaternary Research 19(3):373-387.

Wright, Heather M, Jorge A Vazquez, Duane E Champion, Andrew T Calvert, Margaret T Mangan, Mark Stelten, Kari M Cooper, Charles Herzig and Alexander Schriener

2015 Episodic Holocene eruption of the Salton Buttes rhyolites, California, from paleomagnetic, U-Th, and Ar/Ar dating. Geochemistry, Geophysics, Geosystems 16(4):1198-1210.

Table 1. Summary of infra-red stimulated luminescence (IRSL) dating of Obsidian Butte volcaniclastic sediment from well Union Oil 86-2.

Table 2. Portable X-ray fluorescence (pXRF) data for Obsidian Butte samples 86-2-140.4 (aphyric pumice) and SB0402 (surface obsidian collected adjacent of the well-head), and USGS reference powders for evolved rocks (quartz latite QLO-1; granodiorite GSP-2; certified values from U.S. Geological Survey (2016a).

Figure 1. A) Location map of Obsidian Butte together with major obsidian and fused shale lithic sources for southern California and adjacent regions. B) Digital elevation model of Obsidian Butte showing location of well Union Oil Company of California 86-2. Arrows indicate natural obsidian outcrops around the central dome. Map is based on Light Detection and Ranging (LiDAR) elevation data generated in 2010 which also shows the shoreline at that time (U.S. Geological Survey 2016b).

Figure 2. Stratigraphic well-log of Union Oil 86-2 showing sampled sections and IRSL dates. Vertical black and white bars indicate lithostratigraphic units (from 1 to 3).

Figure 3. Individual post-IR IRSL single grain apparent age estimates for each grain (circles) and the derived sample age (vertical dashed lines and gray band) with one sigma uncertainties. Individual data are shown between 0 and 20 ka (number and range of older dates stated in box) and plotted in rank IRSL sensitivity for each sample with most sensitive grains having the lowest grain numbers. Single grain age estimates included in sample age calculations are shown with solid circles, grains rejected with open circles; see text for details of inclusion criteria. Sample 86-2-148.3 (A) and 86-2-162.8 (B) data show a similar age range, with overlapping depositional ages extracted from the younger data included in age calculations (solid circles). Based on limited crystal availability for core sample 86-2-239.0 (C), the stated age estimate presented is considered tentative.

Figure 4. Ternary representation of Rb, Sr, and Zr abundances in Obsidian Butte aphyric pumice from lithostratigraphic Unit 2 (Sample 86-2-140.4) in comparison to surface obsidian (sample SB0402) and published values (compiled from Shackley 1998, 2017). Compositions for other regional obsidian sources are shown for comparison (Coso: Hughes 1998; Tinajas: Panich et al. 2017).

Figure 5. Summary figure for IRSL eruption age constraints (vertical dashed line and gray band) in comparison with recently published geochronologic data for the Salton Buttes. Approximate extents of major archaeologic periods for the region are only shown for comparison, using definitions given by the Society for California Archaeology (2018).

Table 1. Summary of infra-red stimulated luminescence (IRSL) dating results of Obsidian Butte volcaniclastic sediment from well Union Oil 86-2.

Field code	Lab code	Depth [m]	Chemical composition K wt. % Th µg/g U µg/g	Age [ka]	± [ka]
86-2-148.8	J0468	45.4 140.0	K 2.0 Th 8.5 U 2.93	2.46	0.20
86-2-162.8	J0469	49.6	K 2.2 Th 9.9 U 3.36	2.59	0.27
86-2-239.0	J0470	72.8	K 2.0 Th 6.9 U 2.41	4.39	0.49

± 1-sigma uncertainty

Table 2. Trace element composition of Obsidian Butte lapilli-sized pumice from well Union Oil 86-2 with surface obsidian (SB0402) determined by p-XRF.

Field code/ sample name	Depth [m]	Ti [µg/g]	Rb [µg/g]	Sr [µg/g]	Zr [µg/g]
86-2-140.4	42.8	1172	131	78.2	351
SB0402	surface	1119	141	35.8	350
QLO-1					
Certified		3717	74	340	185
Measured		4065	74	355	230
GSP-2					
Certified		3957	245	240	550
Measured		4060	255	258	701

Reference powders are distributed by USGS; certified values are stated. Zr values for 86-2-140.4 and SB0402 were corrected by a factor of 0.78 based on comparison between measured and reference data. All other elements show deviations <10% relative, and are stated as determined by the instrument software (Thermo Scientific Niton® XL3t GOLDD+ Soil Calibration).

Fig. 1

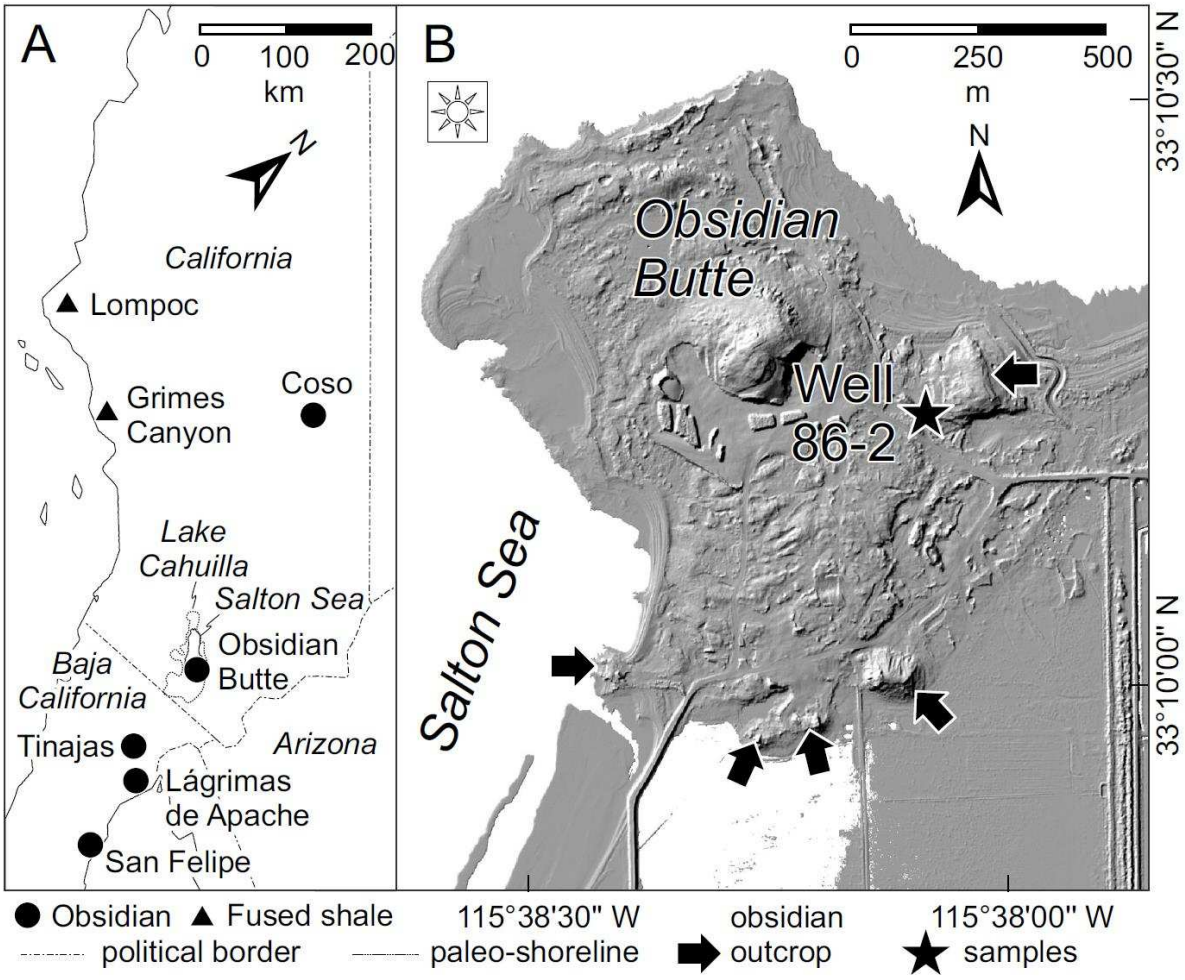
A
0 100 200
km
N
California
Lompoc
Grimes
Canyon
Coso
Lake
Cahuilla
Salton Sea
Obsidian
Butte
Baja
California
Arizona
Tinajas
Lágrimas
de Apache
San Felipe
B
0 250 500
m
N
Obsidian
Butte
Well
86-2
Salton Sea
33°10'30" N
33°10'00" N
115°38'30" W
115°38'00" W
Obsidian
Fused shale
political border
paleo-shoreline
obsidian
outcrop
samples

Fig. 2

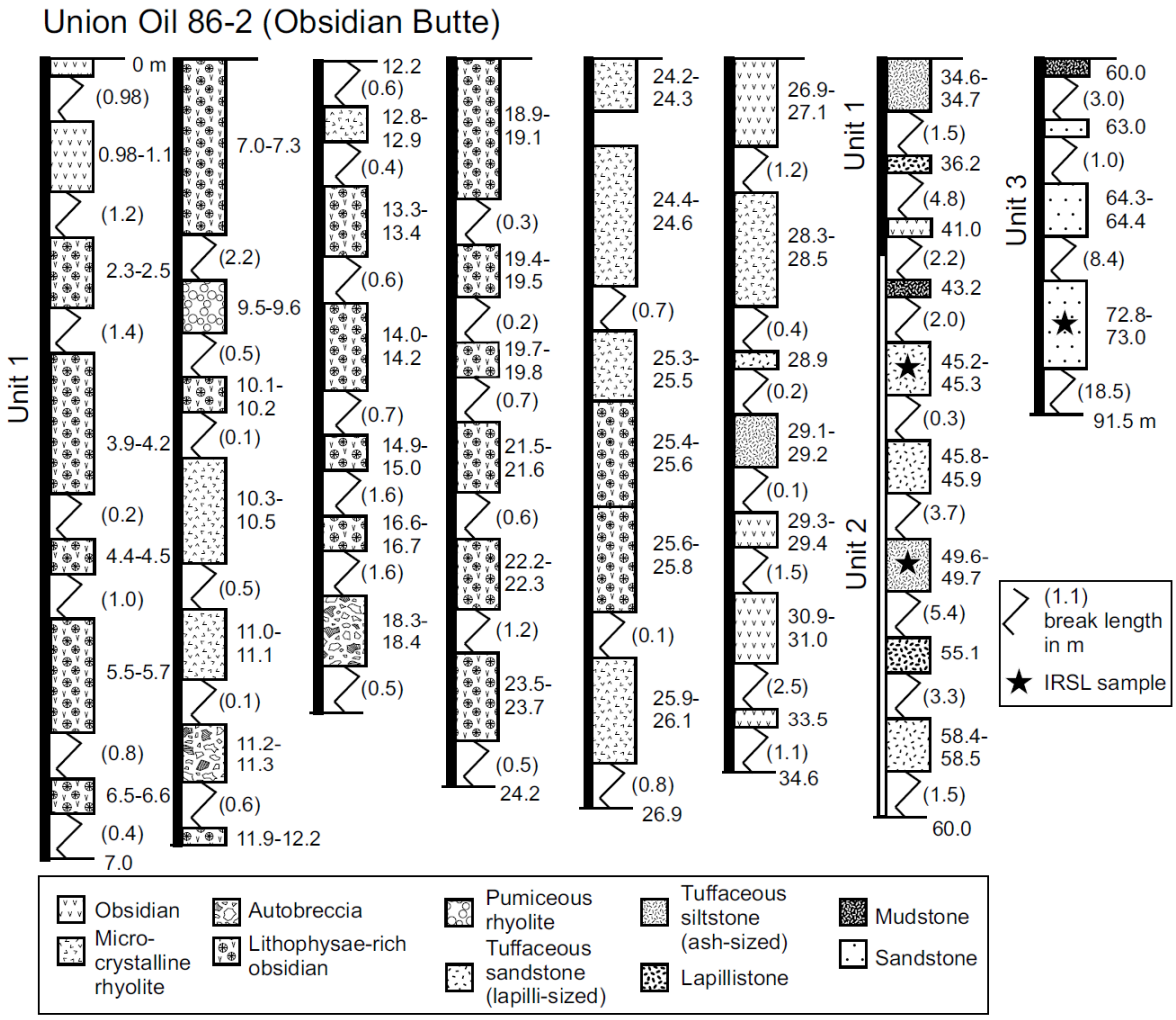
Union Oil 86-2 (Obsidian Butte)
Unit 1
0 m
(0.98)
0.98-1.1
(1.2)
2.3-2.5
(1.4)
3.9-4.2
(0.2)
4.4-4.5
(1.0)
5.5-5.7
(0.8)
6.5-6.6
(0.4)
7.0
7.0-7.3
(2.2)
9.5-9.6
(0.5)
10.1-10.2
(0.1)
10.3-10.5
(0.5)
11.0-11.1
(0.1)
11.2-11.3
(0.6)
11.9-12.2
12.2
(0.6)
12.8-12.9
(0.4)
13.3-13.4
(0.6)
14.0-14.2
(0.7)
14.9-15.0
(1.6)
16.6-16.7
(1.6)
18.3-18.4
(0.5)
18.9-19.1
(0.3)
19.4-19.5
(0.2)
19.7-19.8
(0.7)
21.5-21.6
(0.6)
22.2-22.3
(1.2)
23.5-23.7
(0.5)
24.2
24.2-24.3
24.4-24.6
(0.7)
25.3-25.5
25.4-25.6
25.6-25.8
(0.1)
25.9-26.1
(0.8)
26.9
26.9-27.1
(1.2)
28.3-28.5
(0.4)
28.9
(0.2)
29.1-29.2
(0.1)
29.3-29.4
(1.5)
30.9-31.0
(2.5)
33.5
(1.1)
34.6
Unit 2
34.6-34.7
(1.5)
36.2
(4.8)
41.0
(2.2)
43.2
(2.0)
45.2-45.3
(0.3)
45.8-45.9
(3.7)
49.6-49.7
(5.4)
55.1
(3.3)
58.4-58.5
(1.5)
60.0
Unit 3
60.0
(3.0)
63.0
(1.0)
64.3-64.4
(8.4)
72.8-73.0
(18.5)
91.5 m
(1.1) break length in m
IRSL sample
Obsidian
Micro-crystalline rhyolite
Autobreccia
Lithophysae-rich obsidian
Pumiceous rhyolite
Tuffaceous sandstone (lapilli-sized)
Tuffaceous siltstone (ash-sized)
Lapillistone
Mudstone
Sandstone

Fig. 3

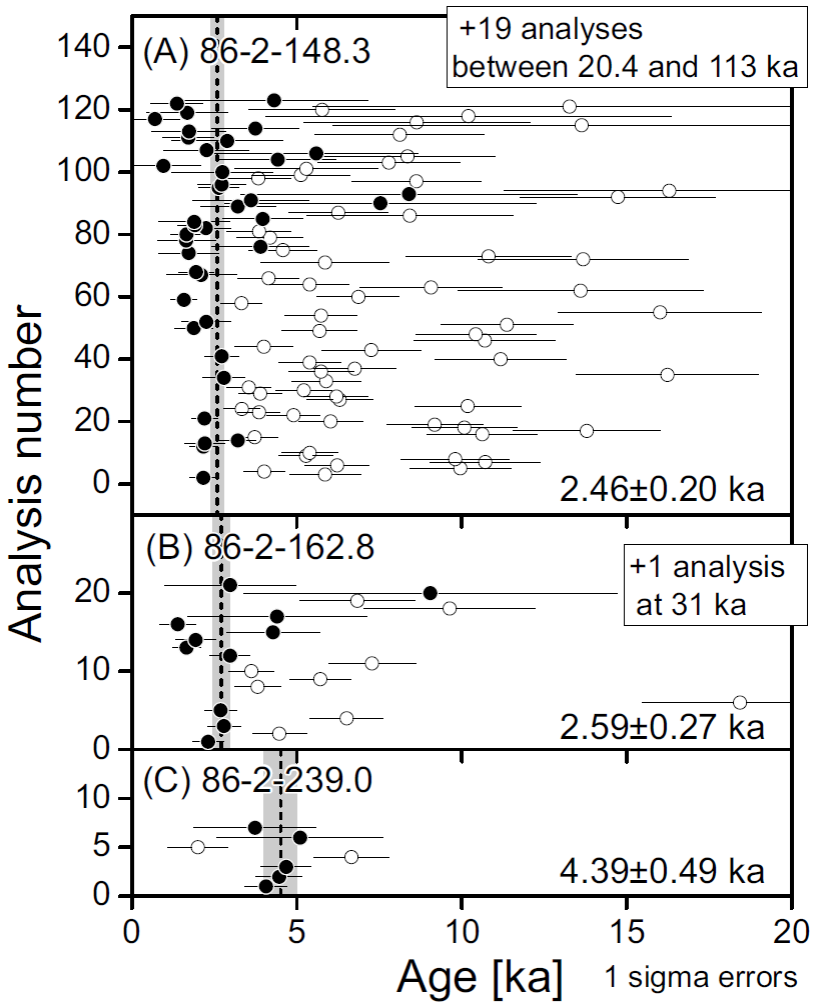
(A) 86-2-148.3
+19 analyses
between 20.4 and 113 ka
2.46±0.20 ka
(B) 86-2-162.8
+1 analysis
at 31 ka
2.59±0.27 ka
(C) 86-2-239.0
4.39±0.49 ka
Analysis number
Age [ka]
1 sigma errors

Fig. 4

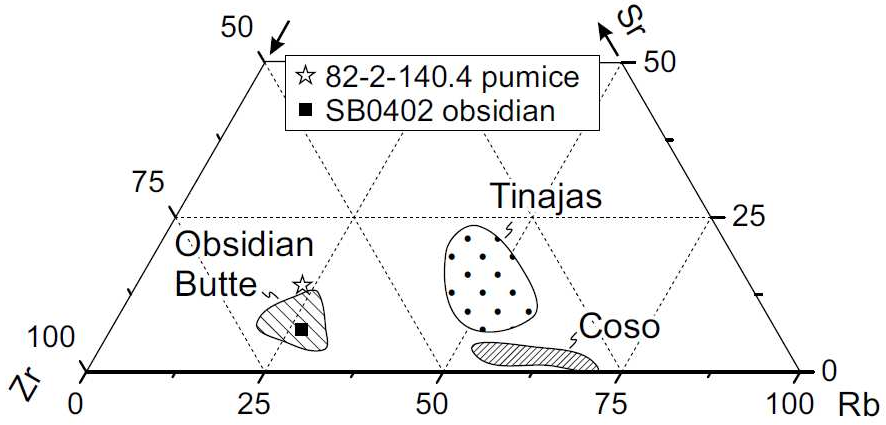
50
Sr
50
☆ 82-2-140.4 pumice
■ SB0402 obsidian
75
Tinajas
25
Obsidian
Butte
100
Coso
Zr
0
0
25
50
75
100
Rb

Fig. 5

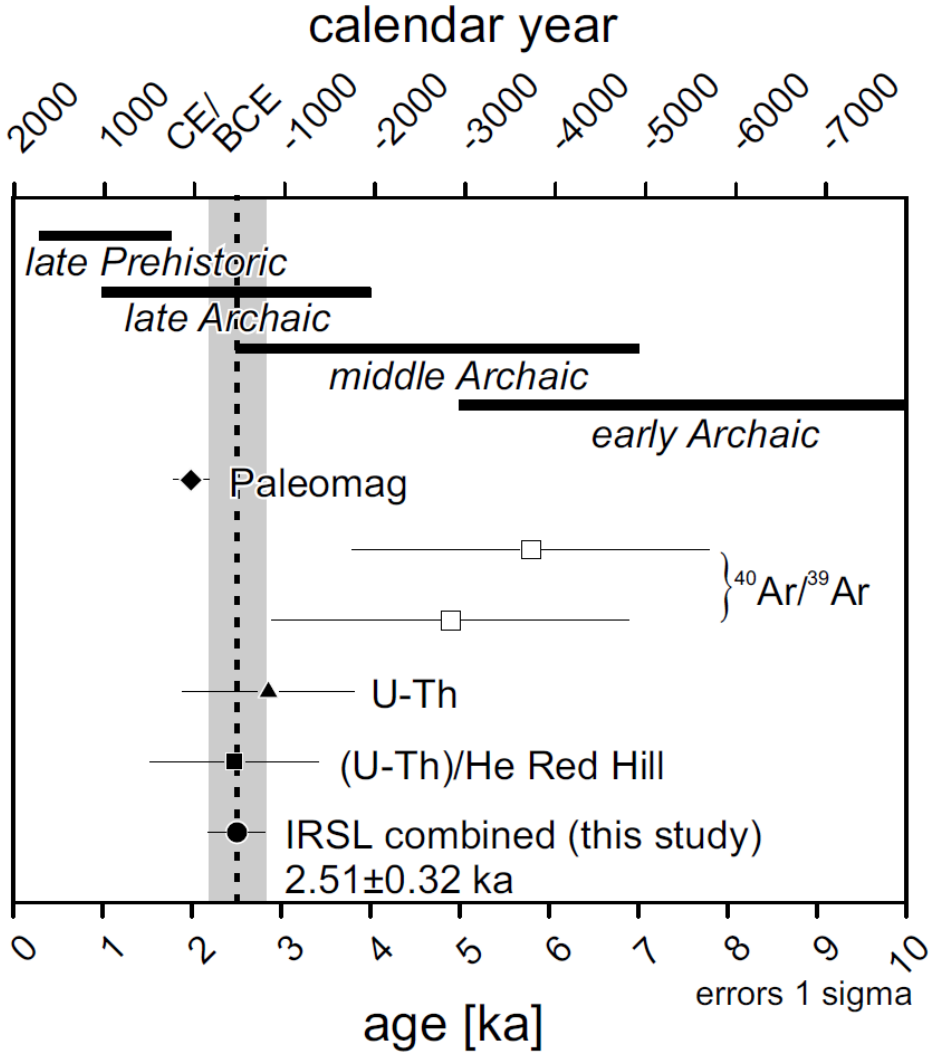
calendar year
2000
1000
CE/
BCE
-1000
-2000
-3000
-4000
-5000
-6000
-7000
late Prehistoric
late Archaic
middle Archaic
early Archaic
Paleomag
40Ar/39Ar
U-Th
(U-Th)/He Red Hill
IRSL combined (this study)
2.51±0.32 ka
0
1
2
3
4
5
6
7
8
9
10
errors 1 sigma
age [ka]